

Supporting information

Experimental

Materials

For the preparation of YTaO_4 , YTaON_2 , $\text{YTa}[\text{ON}\square]_4$, Y_2O_3 (99.99%, Aladdin), Ta_2O_5 (99.0%, High Purity Chemical), KCl (99.8%, Macklin), Mg powder (99.0%, Aladdin), and HNO_3 (65%, Sinopharm Chemical) were used. $\text{H}_2\text{PtCl}_6 \cdot 6\text{H}_2\text{O}$ (>37% Pt, Sinopharm Chemical), $\text{Co}(\text{NO}_3)_2 \cdot 6\text{H}_2\text{O}$ (99.0%, Sinopharm Chemical) were employed as precursors of oxygen evolution cocatalysts. AgNO_3 (99.9%, Sinopharm Chemical) and CH_3OH (99.5%, Sinopharm Chemical) were employed as sacrificial electron acceptors and donors, respectively. La_2O_3 (99.95%, Sinopharm Chemical) was applied as a buffering agent. All chemicals were used as-purchased without further purification.

Synthesize of oxide precursor YTaO_4

The oxide precursor YTaO_4 was prepared by a flux method. Typically, mix the stoichiometric ratio of Y_2O_3 and Ta_2O_5 with the same mass of KCl in a mortar. Then, the mixture was transferred into an alumina crucible and reacted at 1150 °C for 10 h in a muffle furnace. After cooling down, KCl was washed off with deionized water to obtain white powder YTaO_4 .

Synthesize of oxide precursor YTaON_2

The perovskite structure YTaON_2 was synthesized by a nitridation process with Mg assist to enhance the nitridation dynamics. 0.5 g YTaO_4 was mixed with 0.25 g Mg powder in a mortar. Then, it was transferred into an alumina porcelain boat. After removing the air, the powder was nitrided in a stream of 250 mL min^{-1} ammonia gas at 800 °C for 10 h. After removing residual Mg powder and Mg -based compounds in

1 M nitric acid, the perovskite structure YTaON_2 powder was obtained. Nitriding samples at other temperatures were also prepared to observe the phase transition during nitriding.

Synthesis of oxide precursor YTa[ON]_4

The defective fluorite structure YTa[ON]_4 was nitrided by a traditional method. 0.5 g YTaO_4 powder was transferred into an alumina porcelain boat and nitrided in a stream of 250 mL min^{-1} ammonia gas at $1000 \text{ }^\circ\text{C}$ for 10 h. Nitriding samples at other temperatures were also prepared to observe the phase transition during nitriding.

Loading of cocatalysts

The Pt nanoparticles and the CoO_x nanoparticles were loaded on YTaON_2 as the cocatalyst to promote the proton reduction reaction and water oxidation reaction according to previous reports.^{1, 2} PtO_x was loaded on WO_3 as a cocatalyst to promote IO_3^- reduction reaction according to the previous report.³

Characterization

Powder X-ray diffraction pattern (XRD) measurement was carried out on a SmartLab X-ray diffractometer (Cu $K\alpha$ radiation, $\lambda = 1.5418 \text{ \AA}$). High-quality XRD diffraction data were collected for further XRD refinement with a scan rate of 5° min^{-1} per minute and a step size of 0.02° . The scanning range of 2θ is $10\text{-}80^\circ$ and the count for the strongest diffraction peak exceeds 5000. And the Rietveld refinement for XRD was performed on a General Structure Analysis System (GSAS) software.⁴ The surface area was calculated from N_2 adsorption-desorption curve measured at 77 K using a Quadrasorb evo. The morphology and size were observed by a JSM-7900F field emission scanning electron microscope (SEM) and energy dispersive X-Ray Spectroscopy (EDS). X-ray photoelectron spectroscopy (XPS) was performed on an ESCALAB Xi + X-ray photoelectron spectrometer (Al $K\alpha$ X-ray, $h\nu = 1486.6 \text{ eV}$). UV-vis diffuse reflectance spectroscopy (UV-vis DRS) was examined on a Shimadzu

UV2600 with BaSO₄ as background. The thermogravimetric differential thermal analyzer (Diamond TG/DTA) is used to determine the nitrogen content, the atmosphere is air, and the heating rate is 10 °C min⁻¹.

Computational method

All first-principles density functional theory (DFT) calculations were performed with the aid of the Vienna ab initio simulation package (VASP)^{5, 6} based on the projected augmented wave (PAW)⁷ pseudopotentials with cut-off energy of 500 eV. In addition, the generalized gradient approximation (GGA)⁸ with Perdew-Burke-Ernzerhof (PBE)⁹ functional was employed to approximate the exchange and correlation effects during the relaxations. The grids for Monkhorst-Pack¹⁰ *k*-point sampling were 5 × 4 × 5 for YTaON₂. During structure optimizations, the convergence criteria of energy and force convergence threshold on each atom were set to 1.0 × 10⁻⁵ eV and 0.01 eV·Å⁻¹, respectively.

Photocatalytic Performance

The photocatalytic activity was tested on a Pyrex top-illuminated reactor with a 15 °C reflux condensing unit wrapped. For proton reduction half-reaction, 100 mg Pt/YTaON₂ were ultrasonically dispersed 20 vol% CH₃OH. For water oxidation half-reaction, 100 mg CoO_x/YTaON₂ and 100 mg La₂O₃ were ultrasonically dispersed in 10 mM AgNO₃ solution. For Z-scheme overall water splitting, 100 mg Pt/YTaON₂ and 50 mg PtO_x/WO₃ were ultrasonically dispersed in 1 mM KI solution. Before each test, the air was completely removed by pumping for 30 min. The light source comes from a 300 W Xenon lamp with a filter to cut off ultraviolet light ($\lambda \geq 420$ nm) or a band pass filter, which only allows the light of a specific wavelength to pass through. A gas chromatography (GC-2014, Shimadzu) connected to the photocatalyst reactor was utilized to detect the type and the cumulative amount of gas evolved.

Mott-Schottky test

The Mott-Schottky test was carried out on a Princeton electrochemical workstation. For the preparation of the working electrode, 10 mg YTaON₂ powder was dispersed in 1 mL ethanol with 10 μ L 5 wt.% nafion solution, drop it on a piece of 1 \times 2 cm² fluorine-doped tin oxide (FTO) glass. After that, the edge of the FRO glass was covered by glue. A Pt sheet and an Ag/AgCl electrode were employed as a counter electrode and a reference electrode, respectively. The electrolyte is 0.5 M Na₂SO₄ solution.

Results

Table S1 Crystallographic data for YTaON₂ obtained by the Rietveld refinement with reasonable convergence factors ($R_p = 5.53\%$, $R_{wp} = 4.02\%$, and $\chi^2 = 5.417$)

Formula	YTaON ₂
Chemical formula weight	313.87
Crystal system	orthorhombic
Space group	<i>Pnma</i> (62)
a (Å)	5.6676(8)
b (Å)	7.8724(6)
c (Å)	5.5359(4)
α (deg)	90.0
β (deg)	90.0
γ (deg)	90.0
V (Å ³)	246.996(26)
Cell formula units Z	4

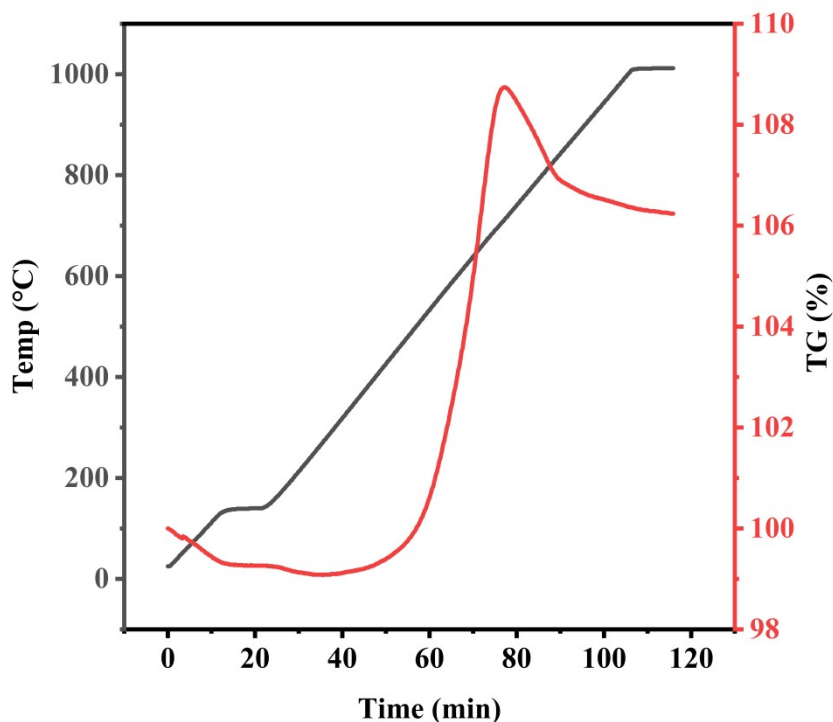


Figure S1. Thermogravimetric analysis for YTaON₂ sample.

In terms of the elemental composition of the prepared sample, Y and Ta are considered to be 1:1 and in a stoichiometric ratio, and the content of nitrogen in the sample is mainly considered. The amount of nitrogen was determined by thermogravimetric analysis (Figure S1). During calcination of the oxynitride under air conditions, there is a stoichiometric replacement of 2 N atoms by 3 O atoms, resulting in a mass gain. As depicted in Figure S1, the mass initially decreases as the temperature increases (below 400 °C), attributed to the desorption of surface adsorbates, moisture, and labile nitrogen. Subsequently, as the temperature rises from 400 °C to 800 °C, the mass first increases and then decreases, corresponding to the process in which oxygen atoms replace nitrogen atoms and nitrogen atoms are not completely removed.¹¹ As the temperature further increases, the nitrogen atoms are further removed and gradually stabilized. The final mass increase is 6.23%, which is very close to the theoretical value of 6.38%. Based on it, the sample is calculated to be YTaO_{1.06}N_{1.94}.

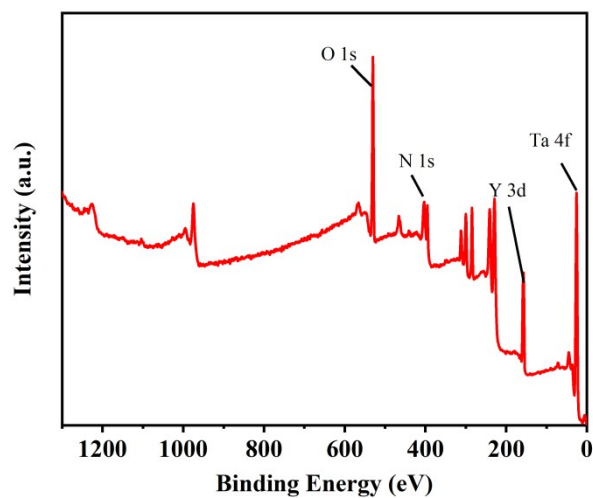


Figure S2. XPS survey spectrum of YTaON₂.

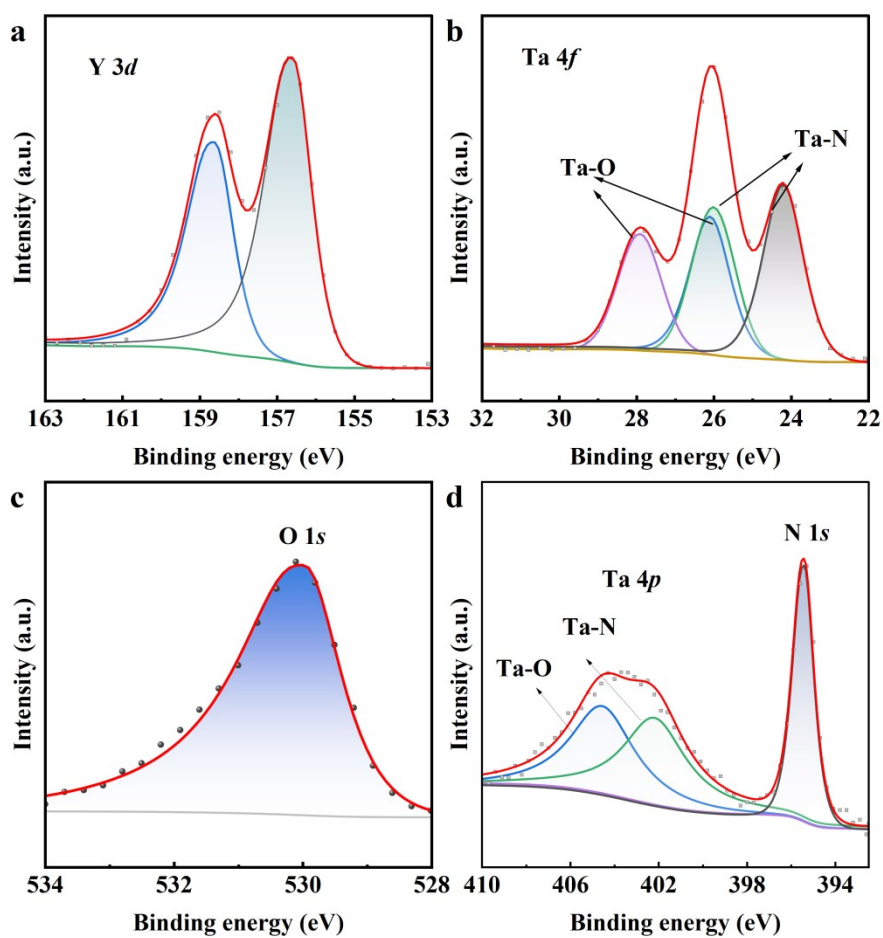


Figure S3. High-resolution XPS spectra of (a) Y 3d, (b) Ta 4f, (c) O 1s, and (d) N 1s.

Table S2. Parameters of the divided peaks of the high-resolution XPS spectra.

Element	Orbital	Binding Energy (eV)	FWHM (eV)	Peak area (cps. eV)
Y	$3d_{5/2}$	156.58	1.43	77734.78
	$3d_{3/2}$	158.61	1.43	53046.41
Ta	$4f_{7/2}$ (a)	26.00	1.32	70807.08
	$4f_{5/2}$ (a)	27.91	1.32	55784.08
	$4f_{7/2}$ (b)	24.19	1.23	93241.29
	$4f_{5/2}$ (b)	26.09	1.23	72238.1
O	$1s$	529.97	1.93	204998
N	$1s$	395.38	1.15	54520.06
Ta	$4p$ (a)	404.51	2.49	35679.84
	$4p$ (b)	402.21	2.54	37406.32

These exact valence states of elements in YTaON₂ were analyzed by X-ray photoelectron spectroscopy (XPS). All of the characteristic peaks of Y, Ta, O, and N elements can be clearly identified in the XPS survey spectrum (Figure S1), implying that these elements coexist in the material. The two peaks located at 156.58 eV and 158.61 eV are ascribed to $3d_{5/2}$ and $3d_{3/2}$ of Y³⁺ (Figure S2a).¹² Besides, these peaks for Ta $4f$ are deconvolved into two groups of peaks by peak fitting. One group peaks locate at 26.00 eV and 27.91 eV are attributed to $4f_{7/2}$ and $4f_{5/2}$ of Ta⁵⁺ in Ta-O and the other ones at 24.19 eV and 26.09 eV results from $4f_{7/2}$ and $4f_{5/2}$ of Ta⁵⁺ in Ta-N (Figure S2b).^{13, 14} Moreover, the peak at 529.97 eV is the characteristic peak of lattice oxygen for O $1s$ (Figure S2c).¹⁵ And the peak at 395.38 eV is the characteristic peak of N $1s$ (Figure S2d),¹⁶ accompanied by the deconvolved peaks at 404.51 eV and 402.21 eV for Ta $4p$ of Ta-O and Ta-N, respectively.

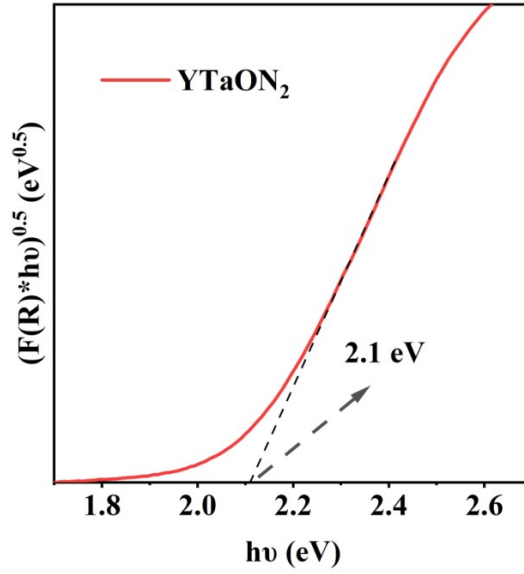


Figure S4. Tauc plots of YTaON₂.

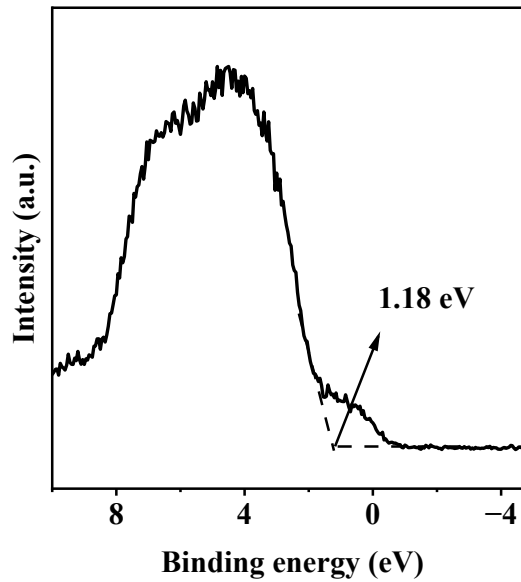


Figure S5. XPS valence spectrum of YTaON₂.

The XPS valence spectrum was further performed to assess the valence band (VB) according to the equation that $E_{\text{VB (vs. RHE)}} = \phi + E_{\text{VB, XPS}} - 4.44$,¹⁷ where the ϕ is the working function of the instrument (4.60 eV) and the $E_{\text{VB, XPS}}$ is the slope intersection in XPS valence spectra. And the VB of YTaON₂ is estimated to be 1.34 eV, which is very close to the results obtained from the results of Mott-Schottky and Tauc plots.

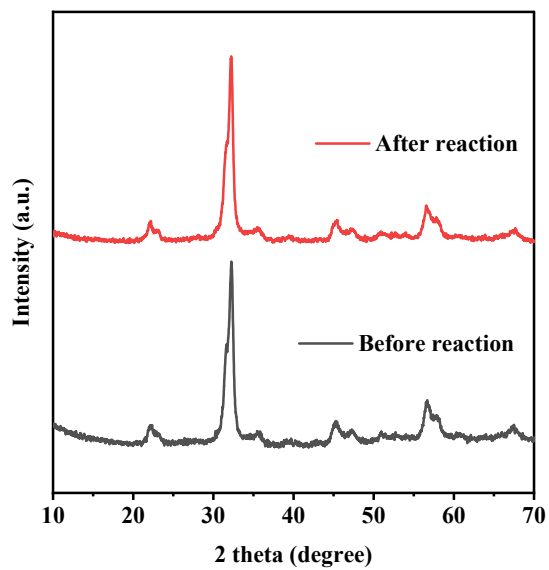


Figure S6. XRD patterns of photocatalyst before and after proton reduction reactions for 5 h.

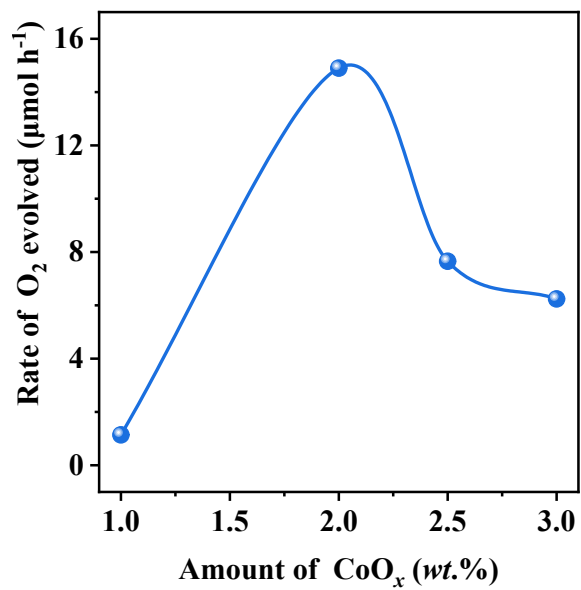


Figure S7. Rate of O₂ evolution as a function of CoO_x loading amount (calculated with metal amount).

Table S3. A list of photocatalytic water splitting performances of representative compounds with a visible light response that were first reported.

Compounds	Absorption edge	Light source	Cocatalyst	Reactant solution	Activity ($\mu\text{mol h}^{-1}$)		Ref.
					H ₂	O ₂	
YTaN ₂ (100 mg)	600 nm	300 W Xe lamp ($\lambda \geq 420$ nm)	1 wt.% Pt	20 vol.% CH ₃ OH	7.2	/	This work
			2 wt.% CoO _x	10 mM AgNO ₃	/	15	
Ta ₃ N ₅ (200 mg)	590 nm	300 W Xe lamp ($\lambda > 420$ nm)	3 wt.% Pt	10 vol.% CH ₃ OH	2.5	/	<i>Chem. Letters</i> 2002 , 31, 736.
			none	5 mM AgNO ₃	/	28 0	
Sr _{1-x} NbO ₃ (100 mg)	650 nm	250 W metal halide lamp ($\lambda \geq 420$ nm)	1 wt.% Pt	25 mM oxalic acid	9	/	<i>Nat. Mater.</i> 2012 , 11, 595.
			none	5 mM AgNO ₃	/	3	
Pb ₂ Ti ₂ O ₅ . 4F _{1.2} (200 mg)	510 nm	300 W Xe lamp ($\lambda > 420$ nm)	0.5 wt.% Pt	TEOA/MeCN (1:13 V/V)	0.2	/	<i>J. Am. Chem. Soc.</i> 2018 , 140, 6648.
			0.5 wt.% RuO ₂	MeCN/H ₂ O (7:3 V/V)	/	trace	
LaTiO ₂ N (200 mg)	600 nm	300 W Xe lamp ($\lambda > 420$ nm)	3 wt.% Pt	20 vol.% CH ₃ OH	12	/	<i>J. Phys. Chem. A</i> 2002 , 106, 29, 6750–6753
			2 wt.% IrO ₂	10 mM AgNO ₃	/	10 0	
g-C ₃ N ₄ (100 mg)	460 nm	300 W Xe lamp ($\lambda > 420$ nm)	3 wt.% Pt	10 vol.% TEOA	10	/	<i>Nat. Mater.</i> 2008 , 8, 76.
			3 wt.% RuO ₂	10 mM AgNO ₃	/	1	
Bi ₂ YO ₄ C 1 (200 mg)	510 nm	300 W Xe lamp ($\lambda > 400$ nm)	5 wt.% Pt	20 vol.% CH ₃ OH	9	/	<i>J. Am. Chem. Soc.</i> 2021 , 143, 6, 2491–2499
			0.5 wt.% (Fe, Ru)O _x	4 mM FeCl ₃	/	18	

BaTaO ₂ N (200 mg)	630 nm	300 W Xe lamp ($\lambda \geq 420$ nm)	3 wt.% Pt	20 vol.% CH ₃ OH	15	/	Solid State Ionics, 2004 , 172, 591 – 595
			none	10 mM AgNO ₃	/	0	
SrTaO ₂ N (200 mg)	600 nm	300 W Xe lamp ($\lambda \geq 420$ nm)	3 wt.% Pt	20 vol.% CH ₃ OH	20	/	Solid State Ionics, 2004 , 172, 591 – 595
			none	10 mM AgNO ₃	/	0	
CaTaO ₂ N (200 mg)	500 nm	300 W Xe lamp ($\lambda \geq 420$ nm)	3 wt.% Pt	20 vol.% CH ₃ OH	15	/	Solid State Ionics, 2004 , 172, 591 – 595
			none	10 mM AgNO ₃	/	0	

References

1. F. Zhang, A. Yamakata, K. Maeda, Y. Moriya, T. Takata, J. Kubota, K. Teshima, S. Oishi and K. Domen, *J. Am. Chem. Soc.*, 2012, **134**, 8348-8351.
2. S. Chen, J. Yang, C. Ding, R. Li, S. Jin, D. Wang, H. Han, F. Zhang and C. Li, *J. Mater. Chem. A*, 2013, **1**, 5651.
3. Y. Miseki, S. Fujiyoshi, T. Gunji and K. Sayama, *Catal. Sci. Technol.*, 2013, **3**, 1750.
4. B. Toby, *J Appl Crystallogr*, 2001, **34**, 210-213.
5. G. Kresse and J. Furthmüller, *Phys. Rev. B*, 1996, **54**, 11169-11186.
6. G. Kresse and D. Joubert, *Phys. Rev. B*, 1999, **59**, 1758-1775.
7. P. E. Blöchl, *Phys. Rev. B*, 1994, **50**, 17953-17979.
8. J. P. Perdew, J. A. Chevary, S. H. Vosko, K. A. Jackson, M. R. Pederson, D. J. Singh and C. Fiolhais, *Phys. Rev. B*, 1992, **46**, 6671-6687.
9. J. P. Perdew, K. Burke and M. Ernzerhof, *Phys. Rev. Lett.*, 1996, **77**, 3865-

3868.

10. H. J. Monkhorst and J. D. Pack, *Phys. Rev. B*, 1976, **13**, 5188-5192.
11. R. Aguiar, D. Logvinovich, A. Weidenkaff, A. Reller and S. G. Ebbinghaus, *Thermochim Acta*, 2008, **471**, 55-60.
12. R. M. Jafer, E. Coetsee, A. Yousif, R. E. Kroon, O. M. Ntwaeaborwa and H. C. Swart, *Appl. Surf. Sci.*, 2015, **332**, 198-204.
13. J. A. Wilks, N. P. Magtoto, J. A. Kelber and V. Arunachalam, *Appl. Surf. Sci.*, 2007, **253**, 6176-6184.
14. R. Fix, R. G. Gordon and D. M. Hoffman, *Chem. Mater.*, 1993, **5**, 614-619.
15. H. Chen and X. Xu, *Appl. Catal. B*, 2017, **206**, 35-43.
16. X. Luo, Y. Xiao, B. Zhang, C. Feng, Z. Fan and Y. Li, *J. Catal.*, 2022, **411**, 109-115.
17. X. Li, B. Kang, F. Dong, Z. Zhang, X. Luo, L. Han, J. Huang, Z. Feng, Z. Chen, J. Xu, B. Peng and Z. L. Wang, *Nano Energy*, 2021, **81**, 105671.